Pergamon

Int. J. Heat Mass Transfer. Vol. 41, No. 10, pp. 1313–1325, 1998

Printed in Great Britain
0017-9310/98 $19.00+0.00

PII: S0017-9310(97)00233-0

Friction, heat and mass transfer for paper drying

S. A. REARDON, M. R. DAVIS and P. E. DOE

Department of Civil & Mechanical Engineering, University of Tasmania, GPO Box 252C, Hobart, Australia 7001

(*Received* 10 *May* 1997)

Abstract—The process of paper drying has been investigated on an experimental basis. The mass transfer coefficient through rough, permeable paper drying fabrics has been shown to be considerably reduced below that from an open surface by between 60–75%, whilst the composition of the paper sheet and increases in felt tension were found to have a minor effect on the observed drying rates (<10%). The turbulence data for the smooth curved hill arrangement supported the prevailing literature in terms of both skin friction coefficient and velocity profiles. The findings of this study have been applied in a mathematical model, relating key operating conditions to achievable drying rates, and highlight the opportunity for the reduction of energy consumption in paper drying. © 1998 Elsevier Science Ltd.

1. INTRODUCTION

In a typical paper machine a number of different dryer fabrics are used throughout the dryer section run. These fabrics vary in permeability and are selected on the basis of their ability to control the amount of air flow exposed to the paper sheet within each dryer pocket. Fabrics with low permeability (75 cfm) are typically selected for use in the wet end of the dryer section where the moisture content of the sheet is relatively high and the sheet strength is therefore low. The low permeability restricts air flow into the dryer pocket and consequently limits sheet disturbance and the possibility of a break.

This variation in the permeability of drying fabrics through the dryer section run prompts questions concerning their varying aerodynamic behaviour. The amount of air dragged by a fabric whilst travelling through the dryer section at speeds of 15–20 m/s is significant from two points of view. Firstly, the boundary layer profile will influence heat and mass transfer from the paper sheet, through the felt and into the hood air. Secondly, the air layer entrained by the fabric is cyclically pumped into and out of dryer pockets as the fabric negotiates the turning rolls. The air currents generated by this process may cause paper sheet instability. Figure 1(a) demonstrates air being entrained by both the dryer fabric and the paper sheet itself. Paper sheet instability resulting from felt-induced turbulence is a complex phenomenon in its own right and is outside the scope of the current study, although it has been addressed previously [1–3].

The drying fabrics also act as a physical impediment to moisture evacuation from the paper sheet. The area restriction the felt imposes on the surface of the paper sheet implies that drying rates over the felt-wrapped cylinders will be substantially less than those in the open draw between cylinders. This aspect of paper

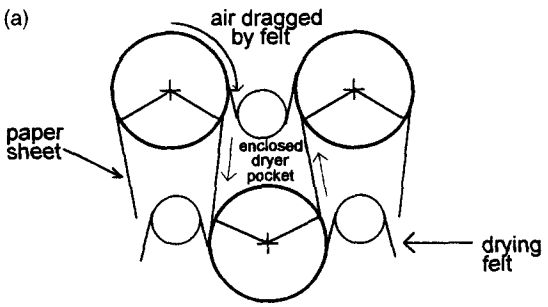

Fig. 1(a). Schematic diagram illustrating air boundary layer development during the paper drying process.

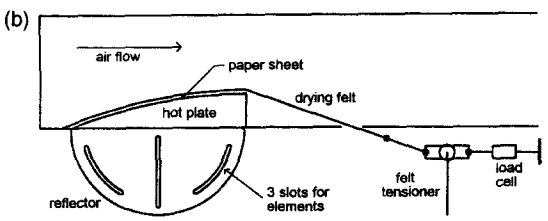

Fig. 1(b). Schematic diagram of laboratory paper drying rig.

drying has attracted limited investigation in the past with most researchers engaged in developing drying models preferring to use the Colburn analogy applied to the open paper surface [4–6]. The intention of this work is to validate the physical properties and conditions that apply in paper drying by carrying out laboratory drying tests. For the paper drying process to be modelled, an unavoidably full range of issues must be considered, as highlighted by Mujumdar [7]. The key specific outcome of this paper is defining the mass transfer coefficient variation for a selection of drying fabrics, whilst taking the opportunity to compare the boundary layer performance of the experimental test facility against the accepted flat plate cor-

relations [8–15] and curved hill investigations carried out on a similarly designed rig [16, 17].

Kirk *et al.* [18–20] have previously noted the difficulty associated with obtaining physical data for the digital simulation of paper machine drying and discussed the need for making arbitrary assumptions. The complexity of the mathematical modelling and the physical environment of the paper machine support this. In this study it is acknowledged that the drying tests carried out are not a perfect simulation of actual machine conditions. However, in the full scale case it is not possible to investigate the detail which is obtainable from a laboratory wind tunnel drying test, and the current objective is to validate the computational drying model in response to key parameters before applying it to an operational paper machine. In this context this paper forms the experimental basis of other work to be published subsequently which will cover in detail the development of a mathematical model for paper drying on a newsprint machine and the comparison between actual machine data and the model simulation results. Reference to this broader work is available in the thesis of Reardon [21] or the paper of Reardon *et al.* [22].

2. EXPERIMENTAL TEST FACILITY

An experimental rig was fabricated for the purpose of conducting a series of paper sheet drying trials and investigating boundary layer development. The testing rig comprised a square sectioned duct (225×225 mm) with radiant electric heating elements positioned beneath a curved aluminium hot plate. The specific geometry of this investigation was selected for several reasons:

- a square hot plate was required to match the size of handsheet samples available (225×225 mm).
- a curved hot plate was necessary to allow the drying fabric (felt), which is a reasonably stiff material, to be tensioned over the hot plate whilst, (a) applying an even pressure over the whole plate, and (b) laying flat at all points so as not to create a bulge which would protrude into the air flow in a different contour to that of the hot plate and paper sheet.
- the radius of curvature of the hot plate of 530 mm was selected to be close to the paper machine drying cylinder radius of 750 mm whilst also allowing the felt to be tensioned adequately with the sample in the wind tunnel and to match the standard handsheet sample dimensions.

The three elements were enclosed by a semi-circular stainless steel reflector that was thermally insulated by a combination of sindayno board and loose fibreglass matting. The hot plate was fitted with nine thermocouples in its top surface. The output from these was monitored by a datalogging computer together with the ambient air temperature and relative humidity.

A piece of dryer fabric was attached to the leading edge of the hot plate. The fabric was drawn over the hot plate and taken out through a downstream slot in the base of the duct. This end of the dryer fabric was then connected to a fixed support by means of a ratchet and turnbuckle arrangement that allowed the fabric to be stretched to a pre-determined tension which was measured by a local cell connected in series with the fabric. A schematic diagram of the test set-up is shown in Fig. 1(b).

Velocity boundary layer measurements were made on three different drying felts. Two of these trials made use of actual paper machine drying fabrics with rated permeabilities of 75 cfm and 350 cfm where cfm is the paper industry ranking in terms of cubic feet per minute of air transmitted through a square foot of the felt under a differential pressure of 1/2″ water gauge. The third trial configuration replaced the felt with a number of nylon lines which were tensioned to hold the paper sheet in place without disturbing the air flow over the smooth curved aluminium surface.

Due to the rough nature of the dryer fabric surface it was difficult to determine a datum for the probe to operate from. The relatively large protrusions of the monofilament polyester weave into the flow demonstrate that the surface datum will necessarily be a somewhat arbitrary definition. This is illustrated by the scanning electron micrographs in Fig. 2. The zero datum was estimated by extrapolating the linear section of the momentum boundary layer profile to a point where the no-slip condition is satisfied. Since velocities as low as $0.1U_\infty$ were able to be measured near the surface the extrapolation is expected to be satisfactory.

A DISA type 55 P01 hot wire probe was used for the boundary layer measurements and as a resistance thermometer enabled the temperature layer to be defined. Comparing this profile with other correlations then enabled the heat flux to be determined. The hot plate temperature was measured with embedded thermocouples and hence the surface heat transfer coefficient was able to be predicted. Results were obtained at a Reynolds number of 2.5×10^5, which corresponds to a flow of 14 m/s through the 225 mm wide duct. The conditions were selected to simulate those used by Australian Newsprint Mills (ANM) in the manufacture of newsprint.

3. BOUNDARY LAYER OBSERVATIONS

(i) *Velocity profile*

The velocity profile for boundary layer air flowing over the dryer felts can be expressed in terms of the wall law relationship. This makes use of the dimensionless parameters u^+ and y^+ which are defined, in accordance with the notation of Schetz [23], as

$$u^+ = \frac{u}{u^*}, \tag{1}$$

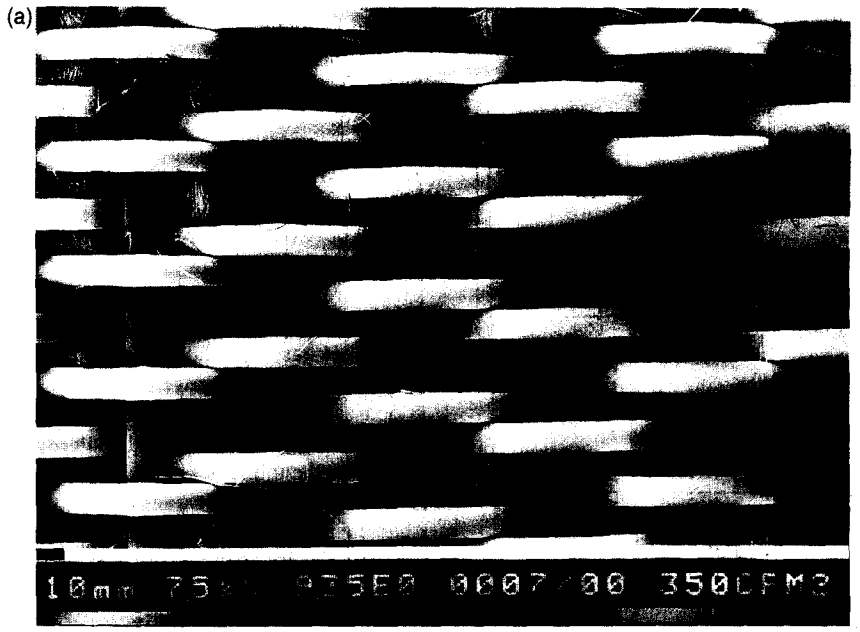

Fig. 2(a). Scanning electron micrograph of a 350 cfm dryer fabric showing surface construction (× 14).

Fig. 2(b). Scanning electron micrograph of a 350 cfm dryer fabric showing edge construction (× 14).

$$y^+ = \frac{yu^*}{\nu}, \tag{2}$$

where friction velocity $u^* = \sqrt{(C_f/2)U_\infty}$, and the remaining variables are fluid velocity (u), free stream velocity (U_∞), distance from the wall (y), and the skin friction coefficient (C_f).

The nondimensional length (y^+) is effectively a Reynolds number and is used as the independent variable in the law of the wall,

$$u^+ = f(y^+). \tag{3}$$

For smooth, flat surfaces the viscous sublayer, $y^+ < 7$, is described by, $u^+ = y^+$, whilst the turbulent inner wall region is generally described by Clauser's (1956) correlation [9],

$$u^+ = 5.6\log(y^+) + 4.9. \tag{4}$$

Figure 3 shows the wall law relationship, $u^+ \sim y^+$, obtained for each of the three axial positions, x, where x is the horizontal distance from the leading edge of the sample, and the normalised axial RMS velocity profile for the various surfaces. The boundary layer thickness, δ, is defined as the point at which the velocity in the boundary layer is 99% of the local free

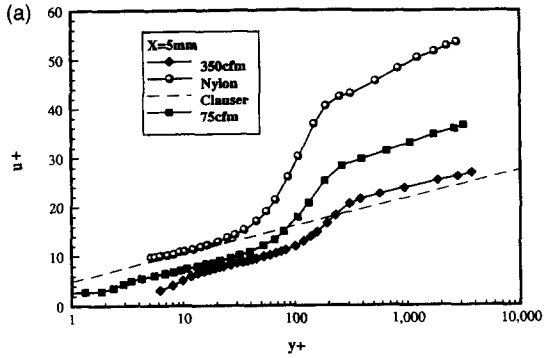

Fig. 3(a). Wall law plot for the three felt arrangements $x = 5$ mm.

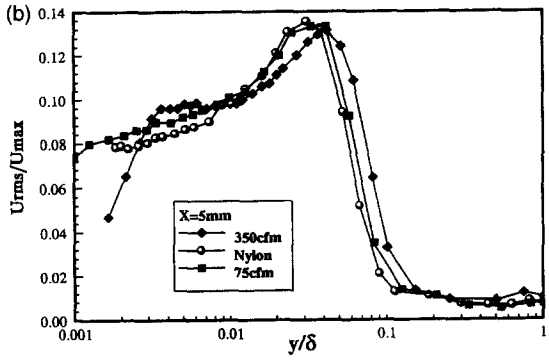

Fig. 3(b). Turbulence intensity plot at $x = 5$ mm.

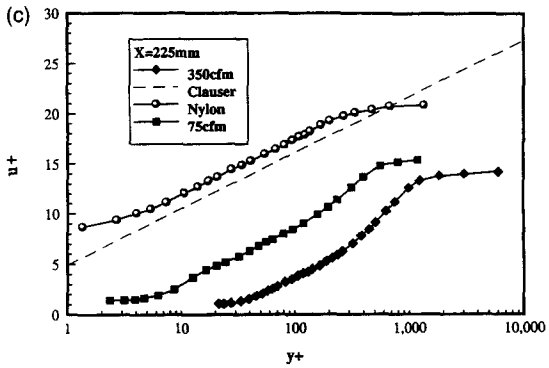

Fig. 3(c). Wall law plot for the three felt arrangements at $x = 225$ mm.

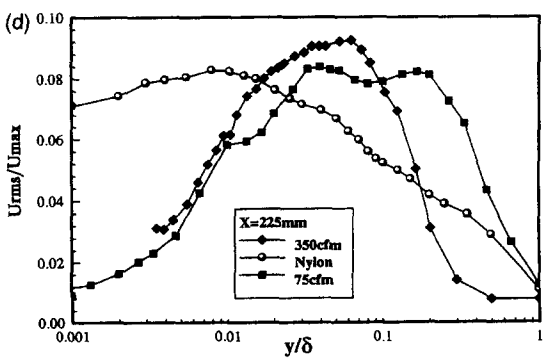

Fig. 3(d). Turbulence intensity plot at $x = 225$ mm.

stream velocity. The wall law plot for the roughened felt surface shows a dual slope characteristic after the initial low turbulence parabolic region which corresponds to the $u^+ = y^+$ region. The inner turbulent layer lies in the approximate range $50 < y^+ < 300$, which varies with the specific test conditions, where the du^+/dy^+ value is independent of surface roughness. The two key differences between the widely documented smooth, flat plate data and the results of this study are surface roughness and the presence of an axial pressure gradient caused by the curved hot plate profile. It has been shown [23, 24] that the inner turbulent flow is insensitive to pressure gradients provided separation is not induced. Thus the wall law plot can be expected to hold for all pressure gradients, except in the immediate area of separation.

Schetz also quotes experimental work which shows that the influence of roughness on the wall law plot is to shift the logarithmic portion of the smooth wall curve down and to the right, corresponding to an increase in C_f. The slope of the logarithmic region does not change. For large k^+ where the laminar sublayer disappears ($k^+ > 70$) the flow is said to be fully rough and the overall effect can be described by [25]

$$u^+ = 5.6\log(y^+) + 4.9 + 5.6\log(k^+) + \Delta, \quad (5)$$

where Δ is a constant and $k^+ = ku^*/\nu$ is the roughness parameter, where k is a measure of the average roughness size. A roughness value ($k = 1$ mm) equal to half the thickness of the dryer fabrics was taken, with the aid of the scale provided on the scanning electron micrographs. The velocity profiles were plotted through using an appropriate value of C_f in the y^+ and u^+ calculations, selected so that the experimental results exhibit the Clauser slope in the internal wall-dominated layer. The resultant skin friction coefficients are listed in Table 1.

Previous investigations [16, 17] by Baskaran *et al.* have demonstrated the growth of an independent internal boundary layer over a curved hill. The internal layer was found to form as a result of the sharp change in surface curvature at the leading edge of the rise and was seen to control the skin friction distribution. The streamwise pressure distributions for Baskaran *et al.* and the geometry of this study are plotted together in Fig. 4(a). The pressure gradient is plotted in terms of the wall pressure coefficient, C_{p_w}, which is defined as

$$C_{p_w} = 1 - \left(\frac{U_{local}}{U_{ref}}\right)^2, \quad (6)$$

where the local and reference upstream velocities are given by U_{local} and U_{ref}, respectively. The two pressure gradient distributions are quite comparable, and this is supported by the fact that the wake factors obtained by Baskaran *et al.* (1987) along the upstream half of the curved hill vary from $\Delta = -4.8$ to $\Delta = +1.0$ in a similar fashion to those for the smooth plate in the current study. As demonstrated in Fig. 4(b) the axial

Table (1a). Skin friction coefficients (C_f), wake factor (Δ) and turbulence intensity data for various drying felt and axial location combinations

Axial location x (mm)	No felt				75 cfm				350 cfm			
	C_f	Δ	U_{rms}/U_{edge}	location (y/δ)	C_f	Δ	U_{rms}/U_{edge}	location (y/δ)	C_f	Δ	U_{rms}/U_{edge}	location (y/δ)
5	0.0007	0.6	13.5%	0.04	0.0015	−7.5	13.5%	0.04	0.0028	−4.7	13.5%	0.04
115	0.0130	−5.0	9%	0.015	0.0190	−10.3	9%	0.02–0.1	0.0360	−12.1	9%	0.02–0.1
225	0.0046	1.4	8%	0.01	0.0085	−3.1	8%	0.02–0.2	0.0100	−12.4	9%	0.03–0.06

Table (1b). Variation in local velocity, wall pressure coefficient, skin friction coefficient, heat flux and surface heat transfer coefficient for the smooth curved hot plate

x (mm)	x/l	U_{local} (m/s)	C_{p_w}	C_f	q_w (W/m^2)	$h_{surface}$ (W/m^2 °C) exp	$h_{surface}$ (W/m^2 °C) Colburn
−12	−0.05	15.94	0.00				
5	0.02	14.91	0.13	0.0007	550	10	8
115	0.51	20.47	−0.65	0.0130	16,610	248	204
225	1.00	25.72	−1.60	0.0046	8900	94	91

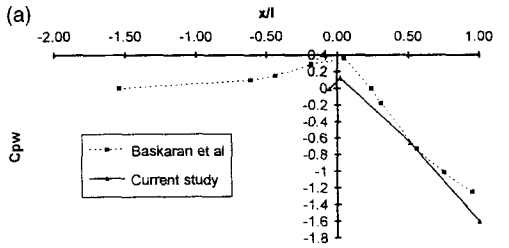

Fig. 4(a). Wall coefficient of pressure C_{p_w}—comparison between Baskaran *et al.* (1987) and the current study.

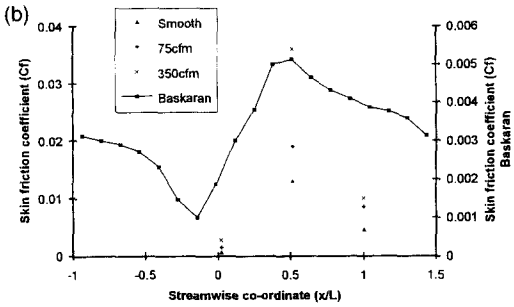

Fig. 4(b). Skin friction coefficient between various drying fabrics and Baskaran *et al.*'s (1987) data for a smooth curved plate.

variation of skin friction coefficient is also generally consistent with the findings of Baskaran *et al.* where C_f is a minimum near the leading edge of the curved hill and increases sharply to a peak at a position 1/3 the distance along the hill profile before decaying slowly near the crest. The highly permeable 350 cfm felt induces more drag than does the 75 cfm felt, attributable to the weave pattern. The 350 cfm felt is more porous and the surface comprises a number of relatively isolated roughness elements as opposed to the denser 75 cfm felt which presents a more uniform surface.

A formal laminar sublayer is not identifiable due to the excessive roughness ($k^+ \cong 60$ for 350 cfm felt at $x = 225$ mm), however, the variation of (U_{rms}/U_∞) for small values of (y/δ) assists in defining zero surface datum for the two rough felts studied. No laminar sublayer was observable in flow over the smooth aluminium hot plate surface with significant turbulence observed to within 20 μm of the wall for each trial.

General literature [23] indicates a maximum axial turbulence intensity of 11.5% for flow over a smooth flat plate at a point which is 1% of the way from the wall to the boundary layer edge. This is generally consistent with the results from the current study with details provided in Table 1. The location and broader spread of the high turbulence zone for the rough dryer fabrics is a consequence of the relatively large dimension scale introduced by the 1 mm roughness elements. Whilst not explicitly detailing turbulence intensity data at small values of (y/δ) Baskaran *et al.* (1987) have a peak intensity of around 10% at entry to the curved hill decreasing to around 6% at the pinnacle of the hill. These values underestimate the data from the current study, but the minor differences in pressure gradients and the concave transition between the flat duct and the inclined hill would account for this. It is noted [16, 17] that turbulence intensity should decrease in areas of favourable pressure gradient, and that the location of the maxima will move towards the edge of the boundary layer as the strength of the pressure gradient increases. This is supportive of the comparison with Klebanoff's flat plate data for which $dp/dx = 0$.

(ii) *Temperature profile*

Kader's [12] correlation for the temperature law of the wall is used to estimate the heat flux through the surface which in turn allows the heat transfer coefficients to be determined. Based on a heat transfer temperature, $T^* = q_w/\rho c_p u^*$, which is analogous to the friction velocity u^*, the dimensionless temperature is $T^+ = (T_w - T)/T^*$. For air with a Prandtl number of 0.7 over the temperature range studied, the logarithmic region may then be expressed by [12],

$$T^+ = 4.88 \log(y^+) + 3.73. \quad (7)$$

Repeating the earlier analogy that the law of the wall applied in spite of differences in pressure gradient and roughness, the T^* value for each trial was manipulated so that the gradient of the internal wall dominated region matched the gradient defined by Kader's correlation.

Figure 5 shows similar axial variation for the temperature and velocity boundary layer profiles for the smooth curved hill with no drying felt. The relativity between the boundary layer profiles at each of the three locations is maintained for both the temperature and velocity relationships. At the peak of the hill the flow is neither accelerating nor decelerating, the pressure gradient is zero. Consequently it is understandable that the velocity and temperature profiles should most closely match the zero pressure gradient, flat plate results at this point. At the initial, $x = 5$ mm, measuring location the pressure gradient has just gone through an abrupt change due to the discontinuity between the duct floor and the leading edge of the curved hill which protrudes into the duct. This sharp favourable pressure gradient causes the large deviation between the measured profiles and the flat plate theory. For the temperature analogy the vertical offset is indicative of a large differential between the wall and flow stream $(T_w - T)$. This implies that the heat transfer will be low which is physically reasonable since the discrete interface between the duct flooring and the hill is expected to promote recirculating eddies which restrict the transfer of heat into the flow.

(iii) *Surface heat transfer coefficient*

The Colburn j-factor analogy for turbulent flow over a flat plate shows the Stanton number to be directly proportional to the skin friction coefficient. Expressing the Stanton number in terms of specific

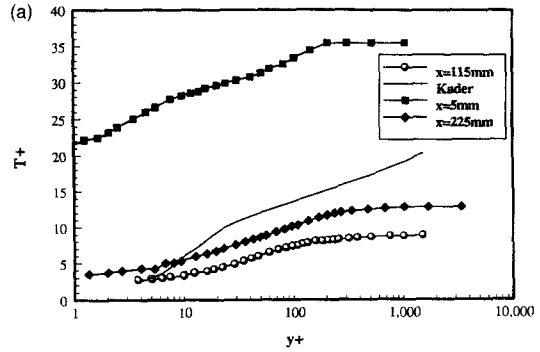

Fig. 5(a). Temperature boundary layer profile at three axial locations for the curved hill with no drying felt compared with Kader's (1981) flat plate correlation.

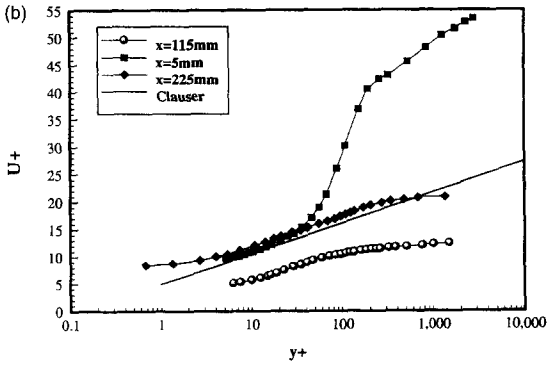

Fig. 5(b). Velocity boundary layer profile at three axial locations for the curved hill with no drying felt compared with Clauser's (1956) flat plate correlation.

heat capacity (c_p), boundary layer edge velocity (u_e) and Prandtl number (Pr) gives the surface heat transfer coefficient,

$$h_s = \frac{\rho u_e c_p}{2Pr^{2/3}} c_f, \tag{8}$$

which is calculated at the three measuring stations. The Colburn analogy underestimates the results of the current study by 18% when the skin friction coefficient is high. Whilst the Colburn analogy is only applicable for zero pressure gradients in laminar flow, in turbulent conditions the analogy is far less sensitive to non-zero pressure gradients [26].

4. DRYING MEASUREMENTS

The experimental rig was designed to dry 225 mm × 225 mm handsheets of paper from an initial moisture content of approximately 5 kg water/kg fibre (80–85% moisture on a wet basis). This is higher than the typical 1.5 kg water/kg fibre moisture content of a paper sheet entering the dryer section of an operational machine, but still allows the drying process to be analysed over the machine range. The wet paper sheet was mounted onto a thin aluminium plate which was contoured to follow the curve of the hot plate surface. These two layers were then sandwiched between the hot plate and drying felt to mark the start of a drying trial. Tensioning of the dryer felt was done manually, threading it through the slot in the bottom of the duct, connecting it to the ratchet device and applying coarse tension before making the fine adjustment using the turnbuckle. The overall arrangement is quite similar to that used by Lee and Hinds [5] in testing 20.3 cm square handsheets of 600 g/m^2 basis weight.

A dynamic sheet-former was used to produce the wet handsheets required for the drying trials. Each handsheet was transferred to individual curved pieces of 0.6 mm aluminium sheeting fabricated specifically for the drying tests performed in this study. The backing plates were shaped to match the contour of the thicker aluminium hot plate in the laboratory drying duct. This facilitated the handling of the very weak wet sheet. The commencement of each drying trial was marked by the removal of the thin backing plate with its attached wet paper specimen from the sealed plastic bag. The specimen plate was weighed, positioned on top of the hot plate and covered with the dryer fabric which was then loaded to the desired tension. Timing of the drying trial began at this point and continued until the fabric tension was released and the sheet removed from the duct for a second weighing (±0.01 g). The sheet was then dried and the moisture content calculated. Average handsheet moisture contents were recorded in all measurements due to the difficulty in partitioning the wet sheet for weighing before drying. Each 225 mm square handsheet was used just once to produce a single datum point on the relevant drying curve of moisture content with time. For each of the drying conditions examined between 8 and 16 data points were used to produce a representative drying curve. The concept of reusing a partially wet sheet in a drying test was dismissed due to the effects of the variation in initial moisture distribution and initial sheet temperature.

Tests were conducted for controlled changes in six major parameters—hot plate temperature, duct air speed, fabric tension permeability, sheet basis weight and sheet furnish composition. The test values were selected on the basis that they cover the range of values relevant to paper machine operation. To handle the combinations a standard drying test was defined and on each occasion just one parameter was varied from this reference point. This gives a total of 18 different drying test conditions. The major results from the drying tests are presented in Fig. 7. All tests were carried out for a sheet basis weight of 50 g/m^2 and a hot plate temperature of 65°C. Each of the 18 distinct drying trials is represented by an exponentially-based best fit curve of the form

$$M = a\exp(b(t+c)^d), \tag{9}$$

where values for a, b, c, and d are presented in Table 2. These smoothed formulations become target drying profiles when input into a computerised algorithm

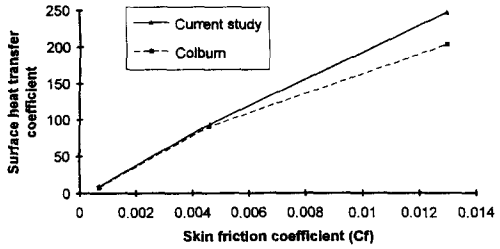

Fig. 6. Linear relationship between C_f and $h_{surface}$.

which seeks to determine the optimal mass transfer coefficient which best matches the observed laboratory drying rate to the prediction of the mathematical drying model of Reardon [21].

A least squares criterion is used for assessing how well the calculated drying curve, generated from a given estimate of mass transfer coefficient, matches the experimentally determined curve. Solving for mass transfer coefficients in this way is a computationally intense procedure. An accelerated searching algorithm was developed to solve for the appropriate value of mass transfer coefficient, h_m. The six groups of results correspond to the variable parameters which feature as part of the experimental drying set-up. The trials conducted for varying surface temperature and sheet basis weight each returned constant values for mass transfer coefficient across a range of values and were used as a base when normalising the experimental results for small variations in these parameters.

(i) *Air flow*

Four tests were undertaken corresponding to free stream air velocities ranging from no flow through to a maximum of 14 m/s over the full duct and 18 m/s as the local peak over the curved hill of the hot plate. An air velocity of 18 m/s simulates a paper machine running at 1080 m/min. This is appropriate as the two paper machines of particular relevance to the wider drying study operate at speeds of 850 m/min through to 1100 m/min depending upon paper grade. The drying rate graphs in Fig. 7 show a maximum departure of data from the best fit curve of 0.23 kg/kg moisture with an average discrepancy of 0.10 kg/kg. The rate of drying is observed to increase with the flow of air over the paper sheet and drying felt.

There are many documented correlations for heat and mass transfer coefficients for flow over a flat plate or over a curved cylinder. The geometry of a curved hot plate in an enclosed duct is midway between the classical flat plate situation and that of cross flow over a cylinder. The variation of mass transfer coefficient with air velocity as depicted in Fig. 8(a) supports this. The flat plate correlation used in Fig. 8(a) is based on Schlicting's (1968) friction coefficient and the Chilton–Colburn (1934) analogy for heat and mass transfer. In terms of the Sherwood number the flat plate correlation is

$$Sh_L = 0.037 Re^{4/5} Sc^{1/3}. \quad (10)$$

In calculating the dimensionless groups the plate

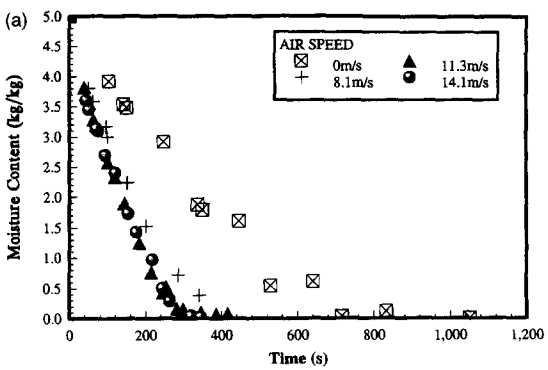

Fig. 7(a). Drying curves for varying air flow.

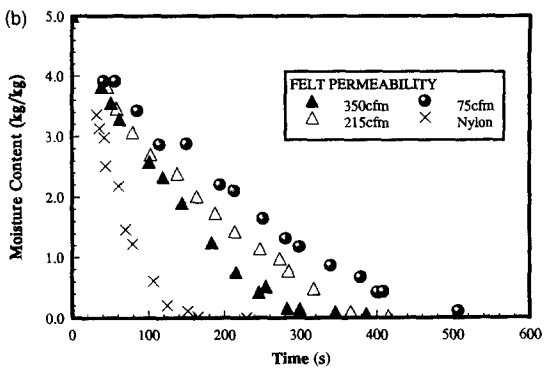

Fig. 7(b). Drying curves for varying felt permeability.

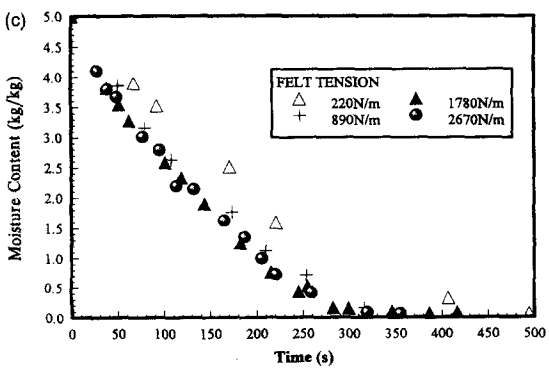

Fig. 7(c). Drying curves for varying felt tension.

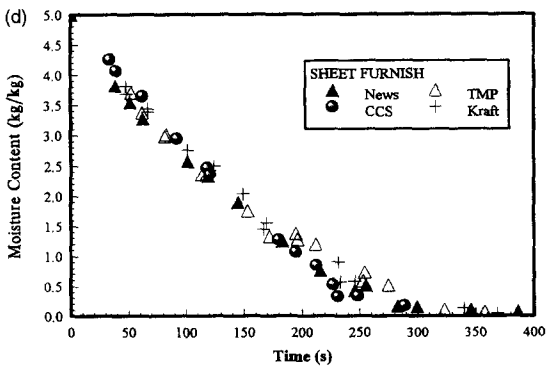

Fig. 7(d). Drying curves for varying sheet furnish.

Table 2. Mass transfer coefficients and best fit parameters for drying curves, $M = a\exp(b(t+c)^d)$

Parameter	Value	Mass transfer coefficient (m/s)	a	b	c	d
Air velocity (m/s)	0	0.0045	6.316	-3.296×10^{-7}	452.4	2.213
	8.1	0.0098	8.340	-3.821×10^{-6}	272.1	2.112
	11.3	0.0126	7.899	-6.275×10^{-8}	294.7	2.791
	14.1	0.0134	7.255	-1.270×10^{-6}	209.1	2.377
Fabric permeability (cfm)	75	0.0078	6.792	-10.30×10^{-6}	208.1	1.959
	215	0.0104	12.01	-4.284×10^{-7}	459.3	2.377
	350	0.0126	7.899	-6.275×10^{-8}	294.7	2.791
	Nylon	0.0303	7.210	-7.445×10^{-8}	149.4	3.079
Felt tension (N/m)	220	0.0134	6.586	-6.583×10^{-7}	183.3	2.488
	890	0.0123	8.061	-1.706×10^{-7}	263.0	2.669
	1780	0.0126	7.899	-6.275×10^{-8}	294.7	2.791
	2670	0.0115	7.056	-5.557×10^{-6}	217.4	2.068
	Mixture	0.0126	7.899	-6.275×10^{-8}	294.7	2.791
Sheet composition	CCS	0.0135	5.480	-7.284×10^{-7}	178.5	2.308
	TMP	0.0114	9.489	-6.395×10^{-6}	230.3	2.119
	Kraft	0.0124	5.885	-11.35×10^{-6}	111.1	2.067

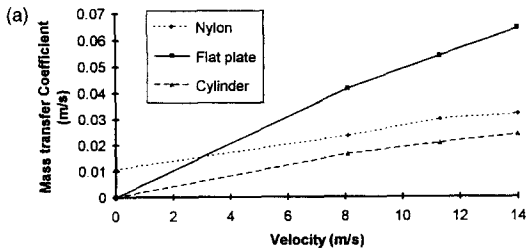

Fig. 8a. Mass transfer correlations for a flat plate and cylinder in cross flow compared with curved hot plate results.

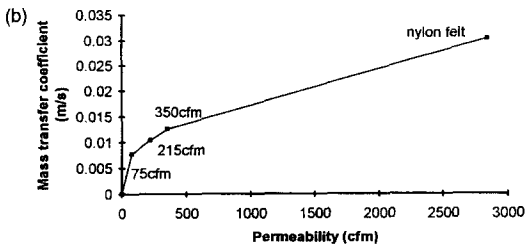

Fig. 8(b). Variation of mass transfer coefficient with felt permeability.

length is 0.225 m. Properties are evaluated at the film temperature, T_f [13],

$$T_f = \frac{T_{plate}+T_{air}}{2}, \tag{11}$$

where, T_{plate} is the surface temperature on the hot plate and T_{air} the temperature of the freestream air flow.

The correlation used for the mass transfer coefficient of a cylinder in cross flow is that of Zukauskas [15],

$$Sh_L = 0.076Re^{0.7}\,Sc^{0.37}\left(\frac{Sc_\infty}{Sc_s}\right)^{1/4}, \tag{12}$$

where the subscript ∞ denotes the free stream and s the surface conditions. This correlation applies for Reynolds numbers in the range from 2×10^5–10^6 and Schmidt numbers less than 10. The Schmidt number is 0.58 whilst the Reynolds number criterion is satisfied for velocities between 3 and 15 m/s. Correlating the observed variation of mass transfer coefficient with air speed for the paper drying experimentation of this study leads to

$$h_m = 0.00159u + 0.011\,[\text{m/s}], \tag{13}$$

where, h_m = mass transfer coefficient, and, u = free stream air velocity. Others to investigate the mass transfer coefficient for the paper drying process include Nederveen *et al.* [6] who use a turbulent model to obtain a theoretical prediction. Nederveen predicts a value of 0.038 m/s for a paper web speed of 10 m/s with no dryer fabric present. This value corresponds to the nylon trial of this study which tensions the paper sheet onto the hot plate while not offering an impediment to mass transfer and predicts a mass transfer coefficient of 0.0300 m/s at a velocity of 11.3 m/s.

Nederveen also quotes the work of Lemaitre (1978) who estimated the mass transfer coefficient to be 0.014 m/s with no dryer fabric at a web speed of 0.8 m/s. This is a very similar situation to the free convection case depicted by the y-intercept on the graph of Fig. 8(a) which suggests a transfer coefficient of 0.011 m/s with zero duct flow.

Others to quote mass transfer coefficients for drying calculations include Harrmann and Schulz [4] and Hartley and Richards [27] who used values of 0.034 m/s and 0.0303 m/s respectively for their simulation of paper drying in the open draw regions. Machine speeds were not quoted in these cases. The constant term in eqn (13) arises for the case of natural convection with zero horizontal duct velocity. This can be estimated using the correlation of Goldstein *et al.*

[28] for mass transfer by natural convection from horizontal flat plates of various geometries. Basing Sherwood and Raleigh numbers on a characteristic length, L^*, defined as

$$L^* = \frac{A}{P}, \tag{14}$$

where A is the plate surface area and P is the perimeter which encompasses the area, Goldstein defined a correlation which universally applied to most flat plate geometries. Those tested included circular, square and rectangular (aspect ratio 7 : 1) plates. For a mass transfer Raleigh number, $Ra_m^* > 200$, the Sherwood number, Sh^*, correlation based on a characteristic length, L^*, was found to be

$$Sh^* = 0.59(Ra_m^*)^{1/4}, \tag{15}$$

where

$$Ra_m^* = \frac{g(\rho_w - \rho_\infty)L^{*3}}{\rho_\infty \nu^2} Sc, \tag{16}$$

and the component terms are gravitational acceleration (g), water vapour concentration at surface (ρ_w), water vapour concentration in surroundings (ρ_∞) and kinematic viscosity of air (ν).

The final calculation shows that Goldstein *et al.*'s correlation predicts a free convection mass transfer coefficient of 0.014 m/s compared to the 0.011 m/s obtained from the correlation resulting from the series of tests. The discrepancy between the experimentally observed free convection mass transfer coefficient and Goldstein's prediction arises from the geometry of the experimental hot plate set-up under test. The curved profile of the test hot plate is clearly a variation of Goldstein's flat plate experimentation. Furthermore, the experimental rig of this study was designed with the principal aim of monitoring forced convection mass transfer and hence the presence of the enclosing ductwork would cause deviations from the correlations developed by others in the area of free convection.

A correlation for free convection mass transfer from an inclined plate of arbitrary angle was obtained by Fujii and Imura [11]. Their results applied to rectangular plates of 6 : 1 aspect ratio and the correlations developed are difficult to apply directly to the current study. However, their results do demonstrate qualitatively that an inclined plate gives rise to a lower transfer rate than does a horizontal plate. Therefore it is reasonable that Goldstein's correlation over-estimates the free convection mass transfer coefficient observed in this study in which the angle of the leading edge of the hot plate from horizontal is 12.5°.

The comparative calculations seek to show how the mass transfer rates of the experimental set-up of this project under varying air velocity are reasonable when considered alongside the more standard and widely repeated physical arrangements documented in the literature. This was found to apply to both forced and free convection situations.

(ii) *Dryer felt permeability*

The four configurations tested included three actual paper machine drying felt samples of differing permeability and a fourth set-up where the drying felt is replaced by a series of nylon tensioning lines. This "nylon" arrangement enables the unimpeded mass flow to be determined and corresponds to the case of a smooth plate. The contact coefficient between paper and hot plate is then unchanged for a given tension but the mass transfer is able to occur without the impediment of the felt. The data relate the vapour transfer impedance provided by dryer felts of various rated permeabilities.

The dryer fabrics are rated in terms of cfm, cubic feet per minute of air passing through a square foot of fabric under a standard pressure differential of 1/2″ water gauge. In these terms the nylon arrangement is designated ∞ cfm. The results demonstrate considerable differences in permissible drying rate. The 75 cfm dryer fabric is seen to slow the drying rate to almost half of the more permeable 350 cfm case. The nylon wire configuration is shown to be twice as conducive to mass flow again. The average scatter for the four curves is below 0.12 kg/kg in each case with the worst of the data points showing a 0.26 kg/kg deviation from the least squares fit.

In Fig. 8(b) the plotting of the 75, 215 and 350 cfm data points is straightforward, however, the equivalent cfm value for the trial with nylon tensioning line (P_∞ cfm) is not immediately apparent. Therefore an estimate was made for the volume flow rate of air (cfm) under the standard conditions of a pressure differential of 0.5″ water gauge (125 Pa) at which the three fabric felts were rated. Bernoulli's energy equation for an ideal fluid represents pressure differential (Δp) in terms of

$$\Delta p = \rho_{water} gh = \tfrac{1}{2}\rho_{air} v^2. \tag{17}$$

The air velocity is the ratio of the volumetric flow rate (Q) and the flow area, 1 ft^2. Hence, the equivalent fabric permeability of the nylon "feltless" tensioning arrangement at 0.5″ water gauge pressure drop is calculated from

$$1000 \times 9.81 \times 0.0127 = \frac{1}{2} \times 1.2 \times \left(\frac{Q}{0.3048^2}\right)^2, \tag{18}$$

whence $Q = 1.34$ m^3/s, or "fabric permeability" = 2840 cfm.

This is included in Fig. 8(b) along with the theoretically extrapolated zero mass transfer at zero permeability. The results indicate a diminishing increase in mass transfer coefficient with increasing permeability, or

$$\frac{\mathrm{d}^2(\text{mass transfer coefficient})}{\mathrm{d}(\text{permeability})^2} < 0. \tag{19}$$

Progressively more permeable felts do not yield proportionally higher drying rates. This effect is important when specifying a particular felt for a given drying duty. The other prime aspect which should also be considered is the effect of air currents passing through a given felt on the stability of the paper sheet. This is a key issue which affects the runnability of the paper machine but is beyond the scope of the current study.

Within the typical range of operating felt permeability (75–350 cfm) the data presents quite smoothly with a steady increase in mass transfer potential for more permeable dryer felts. The 75 cfm sample corresponds to a support felt which would be used in the early stages of the paper machine drying process. The first 6–12 dryer cylinders would be covered by a fabric of this permeability rating. The relatively thick weave fabric prevents excessive air flow from the pocket ventilating ducts being directed onto the wet paper sheet at this point and promoting a sheet break. As the paper dries and its strength increases accordingly the drying fabric permeability is increased at each felt run. This allows progressively more drying air into contact with the paper sheet and consequently improves drying rate. The final dryer sub-section felt is usually rated at around 350 cfm.

Some scanning electron micrographs of a dryer fabric (felt) sample were presented in Fig. 2. These photographs demonstrate the rough nature of the fabric surface. Relatively large gaps are evident between the monofilament polyester weave in the machine direction and the semi-porous cross-directional multifilament members which provide structural rigidity. These interstices allow for the passage of water vapour migrating from the paper sheet. Variations in the weave pattern, filament diameter and spacing influence the felt permeability and surface roughness, which in turn controls air flows in and amongst the dryer pockets.

The nylon tensioning trial which simulates free drying is important for the comparisons it gives with more general heat and mass transfer experimental work performed by others as well as providing information for heat and mass transfer from the free draw section of the paper machine drying run. The open draw is the region of paper sheet running between consecutive drying cylinders. In this region the paper sheet is not supported by the drying fabric but is exposed on both sides to drying air.

(iii) *Dryer felt tension*

The effect of dryer felt tension on paper drying rate was studied over the range from 50 N to 600 N, which was determined as a function of the available equipment and actual paper machine conditions. The tensioning equipment within which the felt was mounted provided a minimum of 50 N tension as a result of the gravitational effects. At the other end of the scale paper machine felts generally operate at 1.7 kN/m_{width} which for the 0.225 m dryer felt under test equates to 385 N. Thus 1.8 kN/m (400 N) was selected as one of the intermediate tension values and 2.7 kN/m (600 N) as an upper bound which extended the testing range whilst staying within the mechanical limits of the system. A 0.9 kN/m (200 N) test made up the fourth felt tension value for this study.

The resultant plots of drying rate are seen to be quite coherent with average deviations from the best fit curves of 0.08 kg/kg and a peak deviation of 0.19 kg/kg. The results demonstrate that dryer fabric tension does influence paper drying rate through improving the contact between the hot plate and paper sheet. However, the effect of increasing fabric tension diminishes at higher values. This is evidenced by the 2.7 kN/m curve drying at a comparable rate with the 1.8 kN/m trial. These results do reinforce the current mode of paper drying with a usual maximum felt tension of 1.7 kN/m_{width}. Further increases in felt tension above this value will only place additional stress on mechanical components and the felts themselves without achieving any significant drying benefit.

Increases in felt tension improve the overall contact between the paper sheet, the thin aluminium backing plate and hot plate, thereby increasing the contact heat transfer coefficient and promoting a higher paper temperature which in turn increases drying rate. The contact heat transfer coefficients, 170, 325, 410 and 430 $W/m^2\,°C$ for felt tensions of 0.22, 0.89, 1.78 and 2.67 kN/m, respectively [21] are input into the computer simulation when optimising for the appropriate mass transfer coefficient for these trials. For constant external conditions, i.e. same dryer felt, air flow and air conditions, the mass transfer coefficient should remain unchanged. The results of Table 2 support this with a maximum variation of 9% about the normal standard value of 0.0126 m/s for the basecase.

The contact heat transfer coefficient data provide a useful basis for analysing the effect of felt tension in a paper machine. The indication is that increased felt tension improves drying rate up to a certain threshold. After this point (400 N ≡ 1.78 kN/m) further increases provide minimal drying benefit and simply increase mechanical strain on the system. This phenomenon has been reported previously in actual paper machine operation. The TAPPI Technical Information Sheet TIS 0404-04 (1989) recommends a dryer felt tension of 1.85 kN/m for a newsprint machine with 1.5 m diameter drying cylinders operating a 1050 m/min. The document notes that beyond this level the gains in heat transfer diminish whilst the higher tensions shorten fabric life, increase bearing loads and drive loads, and cause excessive deflection of fabric rolls. The optimal felt tension is essentially the most economic one when all cost factors are included. It should be emphasised that the TAPPI recommendation is echoed by the tension value applied at ANM and by the point of diminishing returns indicated by comparison between the 400 N (1.8 kN/m) and 600 N (2.7 kN/m) felt tension tests in this study. The experimental results reinforce the TAPPI claim and the ANM practice.

(iv) *Sheet composition*

The effect of sheet composition (furnish) on drying rate behaviour was investigated through experimental with four different handsheets: thermo-mechanical pulp (TMP) made from radiata pine, cold caustic soda pulp (CCS) from eucalypt, an imported softwood kraft and a mixture of the three in the proportion used in newsprint production at ANM, 75 : 20 : 5. The results indicate that varying the pulp furnish has only a mild effect on drying rate. There is a degree of scatter in the results up to a maximum deviation from the best fit curves of 0.22 kg/kg.

The drying rate results for the various pulp furnishes tested are difficult to predict quantitatively without an exhaustive microscopic study and theoretical simulation of fibre size, orientation and bonding characteristics with both similar and dissimilar fibres. Without this parallel study it is not possible to separate the effect of the sheet's internal fibre matrix on drying rate, as determined by the component pulps, from the effct of the surface mass transfer coefficient on drying rate.

The calculated mass transfer coefficients for the four pulp mixtures tested are observed to vary within a relatively small bandwidth. The small deviations between the four samples are brought about by internal drying mechanisms. The configuration of the fibre network specific to reach pulp variety governs the liquid and vapour flow paths within the sheet. Such changes in sheet tortuosity and permeability do influence the drying rate and this effect is perceived as a change in mass transfer coefficient according to the algorithm used for calculation. In summary, the presence of different pulps in comparative trials changes the paper sheet's liquid permeability and vapour diffusivity and since this relationship is not modelled explicitly the calculation method which optimises for just the one variable, interprets the trials as having mildly varying mass transfer coefficients.

With these limitations in mind it is observed that the drying rates vary within a $\pm 10\%$ zone about the mixed furnish (75% TMP, 20% CCS and 5% kraft). The TMP pulp is observed to be the slowest drying of the four combinations tested. It showed a drying rate 9.5% below that of the newsprint furnish which may be regarded as the blended mean. The CCS pulp dries 7% faster than the newsprint whilst the kraft is about 1.5% slower. ANM newsprint is typically made from a blend very similar to the mixed handsheet under test. However, other paper grades which have different strength or appearance requirements use variations in the mixture and this may be significant from the viewpoint of drying rate or drying energy per unit of product. The complicating factor in this forecasting is the differences in the way the three pulps react to the papermaking processes upstream of the dryer section. The twin-wire former and press section are essentially dewatering processes which are extremely dependent upon the structure of the paper sheet fibre network. The experiences of paper machine operators suggests that CCS makes the greatest demands on the drying energy required whilst kraft requires considerably less. Such differences are not a result of the weak variations in drying behaviour for the various pulps but rather considerable differences in the forming and pressing characteristics of these materials. For example, with all other parameters unchanged, a CCS-rich paper sheet will have a higher initial moisture content at entry to the dryer section. This increases the dryer section energy requirement and makes CCS appear to be a slow drying pulp.

The difficulty with supporting these arguments with actual paper machine drying data arises from the absence of an on-line moisture content analyser between the press and dryer sections on the paper machine under test. This means that the inlet paper sheet moisture content is logged on a monthly basis only by manual sampling prior to a planned machine maintenance shutdown. Consequently there is no real-time feedback between pulp furnish and drying behaviour. A Measurex scanner records the moisture profile of the sheet as it leaves the dryer section and this information provides the key input for dryer section control. Such scanners are very expensive and multiple scanners are rarely installed as operating experience has often shown them to be relatively unreliable in the hot and wet conditions prior to the dryer inlet. Recently, however, gamma gauges are now being used for measuring drying profiles along the machine.

To summarise, the drying rate differences evident for different pulps are firstly relatively minor with each of the individual pulp lying within a $\pm 10\%$ band about the typical newsprint furnish. Secondly, adjustments to the theoretical drying rate predicted by the model can be made for variations on the pulp furnish but these calculations will only be useful if information pertaining to the initial moisture content at dryer section entry is known and input into the model.

5. CONCLUSIONS

The mass transfer coefficient through rough, permeable paper drying fabrics has been shown to be considerably reduced below that from an open surface by between 60–75% depending upon the permeability ratings of the fabric. Mass transfer from the free surface of the curved hill was also analysed and found to lie between that for flow over a flat plate and for a cylinder in cross-flow. For the free convection case the mass transfer coefficient was found to underestimate the flat plate prediction by 21%.

From an applied viewpoint, the drying data illustrated that the tension of the machine drying fabrics is maintained near an optimal point of 1.8 kN/m, above which there is negligible improvement in drying rate to counteract the reduced mechanical life of the components. Drying rates from a range of component pulps were found to differ by less than 10%, contrary to the perception of those involved in the paper industry, the conflict being explained by upstream dewatering processes which lead to a moisture content at

dryer section inlet based on pulp composition and sheet fibre structure.

The turbulence data for the smooth curved hill arrangement were examined alongside similar experimental arrangements [16, 17]. Under almost identical pressure gradients, the two arrangements exhibited similar trends in skin friction coefficient. The velocity profiles were analysed against the literature and found to be generally consistent with peak turbulence intensity values between 8–13% occurring at locations from 0.01–0.04 (y/δ).

The findings of this study have been applied in a mathematical model which describes paper drying on a newsprint machine, relating key operating conditions to achievable drying rates [21]. The results have application in optimising the drying conditions and dryer section geometry of the paper machine for the reduction of drying energy consumption.

REFERENCES

1. Soininen, M. and Nurminen, J., An orientation to the pocket ventilation design in a drying section with open mesh fabrics. *Paperi ja Puu*, Vol. 4a, 1974.
2. Soininen, M., The physics of paper machine sheet flutter. *International Water Removal Symposium*, 1982, pp. 85–86.
3. Fagerholm, L., Thermodynamical properties of dryer fabrics for high speed paper machines. *1990 Tappi Engineering Conference*, pp. 165–174.
4. Harrmann, M. and Schulz, S., Convective drying of paper calculated with a new model of the paper structure. *Drying Technology*, 1990, **8**(4), 667–703.
5. Lee, P. F. and Hinds, J. A., A technique for measuring the drying characteristics of fiber webs. *Tappi Journal*, April 1979, **62**(4), 45–48.
6. Nederveen, C. J., Van Schaik-Van Hoek, A. L. and Dijkstra, J. J. F. M., Present theories on multi-cylinder paper drying. *Paper Technology*, November 1991, pp. 30–35.
7. Mujumdar, A. S., *Handbook of Industrial Drying*. Marcel Dekkar, 1995, pp. 849–898.
8. Chilton, T. H. and Colburn, A. P., Mass transfer (absorption) coefficients—prediction from data on heat transfer and fluid friction. *Industrial and Engineering Chemistry*, 1934, **26**, 1183–1187.
9. Clauser, F. H., *Advances in Applied Mechanics—Vol. IV*. Academic Press, New York, 1956.
10. Colburn, A. P., A method of correlating forced convection heat transfer data and a comparison with fluid friction. *Transactions of the American Institute of Chemical Engineers*, 1933, **29**, 174–210.
11. Fujii, T. and Imura, H., Natural convection heat transfer from a plate with arbitrary inclination. *International Journal of Heat and Mass Transfer*, 1972, **15**, 755–767.
12. Kader, B. A., Temperature and concentration profiles in fully turbulent boundary layers, *International Journal of Heat and Mass Transfer*, 1981, **24**, 1541–1544.
13. McAdams, W. H., *Heat Transmission*. McGraw-Hill, 1985.
14. Schlicting, H., *Boundary Layer Theory*, 6th edn. McGraw-Hill, New York, 1968.
15. Zhukauskas, A., Heat transfer from tubes in cross-flow. *Advances in Heat Transfer*, Vol. 8, Academic Press, New York, 1975.
16. Baskaran, V., Smits, A. J. and Joubert, P. N., A turbulent flow over a curved hill. Part 1. Growth of an internal boundary layer. *Journal of Fluid Mechanics*, 1987, **182**, 47–83.
17. Baskaran, V., Smits, A. J. and Joubert, P. N., A turbulent flow over a curved hill. Part 2: effects of streamline curvature and streamwise pressure gradient. *Journal of Fluid Mechanics*, 1991, **232**, 377–402.
18. Kirk, L. A., Digital simulation of the effect of operating and design variables on the dryer section of a paper machine. *Paper Technology and Industry*, 1980, **21**, 61–71.
19. Kirk, L. A. and Jones, G. T., Hot surface drying of paper. *Paper Technology*, 1970, **11**, 347–352, 397–403.
20. Kirk, L. A., Hudson, F. L. and Hearle, J. W. S., Mechanism of moisture transfer to felt during hot surface drying. *Paper Technology*, 1963, **4**, 251–257.
21. Reardon, S. A., Simulation of paper drying energy consumption. Doctoral Thesis, University of Tasmania, 1994.
22. Reardon, S. A., Davis, M. R. and Doe, P. E., Effect of heat and mass transfer on the performance of paper making machines. *6th Australasian Heat and Mass Transfer Conference*. Sydney, December 1996.
23. Schetz, J. A., *Foundations of Boundary Layer Theory for Momentum, Heat and Mass Transfer*. Prentice-Hall, Englewood Cliffs, N.J., 1984.
24. Ludwieg, H. and Tillmann, W., Investigation of the wall shearing stress in turbulent boundary layers, NACA TM 1285, 1950 (abstract).
25. Hama, F. R., Boundary layer characteristics of smooth and rough surfaces. *Trans. Soc. Nav. Arch. Mar. Eng.*, 1954, **62**, 333–358.
26. Incropera, F. P. and Dewitt, D. P., *Fundamentals of Heat and Mass Transfer*. John Wiley and Sons, 1985, pp. 334–335 and 777.
27. Hartley, F. T. and Richards, R. J., Hot surface drying of paper—the development of a diffusion model. *Tappi Journal*, March 1974, **57**(3), 157–164.
28. Goldstein, R. J., Sparrow, E. M. and Jones, D. C., Natural convection mass transfer adjacent to horizontal plates. *International Journals of Heat and Mass Transfer*, 1973, **16**, 1025–1035.